ORIGINAL ARTICLE

Comparison of Strain-Encoding and Feature-Tracking Derived Myocardial Deformation Assessment of Left Ventricular Function in a Pediatric and Adult Congenital Heart Disease Cohort

Joshua D. Chew[1] · Kristen George-Durrett[1] · Benjamin Acheampong[1] · Jeffrey G. Weiner[1] · James C. Slaughter[2] · David A. Parra[1] · Jonathan H. Soslow[1]

Abstract

Background Cardiac magnetic resonance (CMR) strain can be assessed with feature-tracking (FT), which utilizes a post-processing algorithm to quantify myocardial deformation on routine cine images, and strain-encoding magnetic resonance imaging (SENC), which uses parallel magnetization tags combined with out-of-plane phase-encoding gradients to quantify deformation. Assessing agreement is critical to determine whether results can be translated between methods. We compared SENC to FT in the assessment of left ventricle (LV) global longitudinal strain (GLS) and global circumferential strain (GCS) in a cohort of pediatric and adult congenital heart disease (ACHD) patients.

Methods Pediatric subjects and ACHD patients underwent CMR on 1.5 T Siemens scanners, including balanced steady-state-free precession (bSSFP) cine imaging and SENC acquisitions in apical two and four chamber, left ventricular outflow tract, and short axis views. bSSFP cine imaging FT analysis was completed with Medis QStrain. Myocardial Solutions MyoStrain was used to analyze SENC. Correlation was assessed by Spearman's rank correlation coefficient. Agreement between techniques was assessed with concordance correlation coefficient (CCC) and Bland–Altman.

Results The cohort included 134 patients, 75 with congenital heart disease (56%). The median age was 16.3 years (IQR 13.7, 19.5). Median LV ejection fraction was 57% (IQR 54.4, 61.6). SENC and FT were in poor agreement for GLS (Spearman's $\rho = 0.58$, $p < 0.001$; CCC 0.24) and GCS (Spearman's $\rho = 0.29$, $p < 0.001$; CCC 0.03).

Conclusion There was poor agreement between SENC and FT derived GLS and GCS in a cohort of pediatric and ACHD patients, suggesting that SENC and FT cannot be used interchangeably.

Keywords Cardiac magnetic resonance · Myocardial deformation · Strain · Pediatric · Adult congenital heart disease

Abbreviations

ACHD	Adult congenital heart disease
A2C	Apical two chamber
A4C	Apical four chamber
bSSFP	Balanced steady-state-free precession pulse sequence
CMR	Cardiac magnetic resonance
DENSE	Displacement-tracking with stimulated echoes
EDV	End diastolic volume
ESV	End systolic volume
EF	Ejection fraction
FT	Feature-tracking
GCS	Global circumferential strain
GLS	Global longitudinal strain
HARP	Harmonic phase magnetic resonance
LGE	Late gadolinium enhancement
LV	Left ventricle
LVOT	Left ventricular outflow tract
PSIR	Phase-sensitive inversion recovery
SAX	Short axis
SENC	Strain-encoding magnetic resonance imaging

✉ Joshua D. Chew
joshua.d.chew@vumc.org

1 Division of Pediatric Cardiology, Department of Pediatrics, Vanderbilt University Medical Center, 2200 Children's Way, Suite 5230, Doctor's Office Tower, Nashville, TN 37232, USA

2 Department of Biostatistics, Vanderbilt University Medical Center, Nashville, TN, USA

Background

Myocardial deformation imaging with the quantification of strain has emerged as an important technique in the assessment of cardiovascular diseases. Alterations in strain have been shown to precede reductions in ejection fraction and associate with major adverse cardiac events, including mortality [1–7]. Cardiac magnetic resonance (CMR) quantification of strain can be performed in many ways. Feature-tracking (FT) is a post-processing technique that allows the quantification of strain from standard CMR cine images. FT depends on the identification of specific regions of tissue on a frame-by-frame basis throughout the cardiac cycle [8]. Strain-encoding magnetic resonance imaging (SENC) is a method that utilizes magnetic tagging of different regions of the myocardium. SENC uses pulse sequences to apply magnetization tags parallel to the image plane in addition to orthogonal phase-encoding gradients to compute strain [9].

Each technique is intrinsically different and therefore has unique strengths and weaknesses impacting its feasibility and utility in clinical care. The major benefit of FT is the accessibility and ease of use with the utilization of cine images that are acquired as part of standard clinical scans and the several commercially available software options. However, the availability of several software options also leads to a lack of standardization of analysis algorithms across vendors and less validation data. Additionally, FT relies on proprietary algorithms to identify image "features" within prescribed contours, rather than intra-tissue markers. SENC, meanwhile, is a technique that provides high spatial resolution and short acquisition times with fast post-processing for the quantification of longitudinal and circumferential strain. But SENC suffers from the need for technique specific requirements including specific sequences that need to be acquired in addition to standard imaging protocols, as well as specialized software for analysis [10].

Based on the inherent differences of the imaging techniques, as well as software-related factors, there is the potential for significant differences between strain quantification methods [10]. Image acquisition factors, including spatial and temporal resolution, image quality, and accuracy of standardized image view, can lead to variation in resultant strain calculations. Additionally, it is unclear the extent to which strain derived from different imaging techniques, such as harmonic phase (HARP) analysis of tagged images, displacement-tracking with stimulated echoes (DENSE), SENC, and FT, may correlate to allow for interchangeability [11–17]. These differences must be understood before strain can be adopted for clinical management. The objective of the study was to investigate the agreement between SENC and FT in the measurement of left ventricular (LV) global longitudinal strain (GLS) and global circumferential strain (GCS).

Methods

Study Population and Design

The study retrospectively evaluated patients and healthy volunteers who underwent CMR imaging from October 22, 2018 to February 10, 2020. Inclusion criteria were all subjects less than 18 years of age regardless of diagnosis and subjects 18 years of age or older with a diagnosis of congenital heart disease who underwent CMR. Subjects were excluded if the appropriate imaging sequences were not obtained or if image quality precluded analysis. Of note, in addition to patients undergoing clinically indicated CMR, ten healthy pediatric controls who underwent CMR during the included time period for a separate study determining laboratory normative data were included in the analysis. For all pediatric subjects, guardians provided informed consent and the subject provided assent. All adult subjects provided informed consent. The study was approved by the Vanderbilt University Medical Center Institutional Review Board.

A total of 248 subjects underwent CMR during the study period and a total of 134 subjects were included in the analysis (Fig. 1). There were 89 pediatric subjects and 45 adult subjects with congenital heart disease. The cohort was predominantly male with primarily adolescents and young adults (Table 1).

Image Acquisition

Images were acquired on a 1.5 T scanner (Siemens Avanto with 8 channel phased array cardiovascular coil and Avanto Fit with 32 channel phased array cardiovascular coil). A balanced steady-state free precession pulse sequence (bSSFP) was used to obtain retrospectively gated cine images in the apical two chamber (A2C), left ventricular outflow tract (LVOT), apical four chamber (A4C), and short axis (SAX) views. SAX slices were obtained covering the LV from base to apex (8 mm thickness, 0 mm gap). Typical scanning parameters were: TR = 36.53 ms, TE = 1.18 ms, flip angle 80°, voxel size $1.5 \times 1.5 \times 8$ mm, 25 phases. SENC images were obtained in the A2C, LVOT, A4C, and three SAX slices (base, mid-ventricle, and apex). Typical scanning parameters were: TR = 35.21 ms; TE = 1.33 ms; slice thickness = 12 mm; signal averages = 1, concatenations = 1, phase oversampling = 0%, distance factor = 20%, voxel size $– 4.7 \times 4.7 \times 12$ mm, 13–25 phases. The CMR technicians performing the studies were trained and certified by Myocardial Solutions in the use of SENC imaging.

A subset of the cohort underwent late gadolinium enhancement (LGE) imaging based on clinical indication and discretion of the cardiologist supervising the CMR. Subjects undergoing LGE imaging received
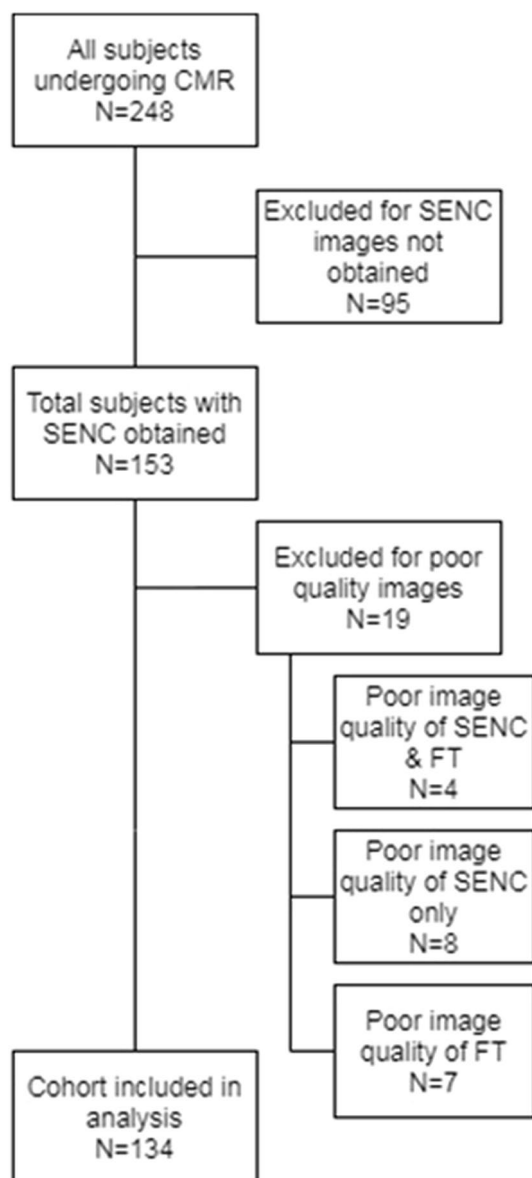
Fig. 1 Flow chart of the study population. Cardiac magnetic resonance (CMR); strain-encoding magnetic resonance imaging (SENC); feature-tracking (FT)

0.15–0.2 mmol/kg gadobutrol (Gadavist, Bayer Health-Care Pharmaceuticals) via a peripheral intravenous catheter. Imaging was performed 10 min after contrast administration per laboratory protocol, with the majority undergoing both a phase-sensitive inversion recovery sequence (PSIR) and inversion recovery-prepared true fast imaging with steady precession (TrueFISP) in the SAX view covering the LV from base to apex.

Baseline Characteristics

Baseline characteristics, including sex, age, height, weight, heart rate, and blood pressure, as well as primary cardiac diagnoses were collected from a prospectively maintained database for all patients undergoing CMR at our center. Conventional LV parameters, including indexed end-diastolic volume (EDV), indexed end-systolic volume (ESV), and ejection fraction (EF), were collected from the CMR database. These parameters were measured by pediatric cardiologists *(J.D.C., D.A.P., J.H.S.)* experienced in CMR as part of clinical care or during enrollment of control subjects. EDV, ESV, and EF were measured by manual planimetry of the endocardium, with inclusion of the papillary muscles, in a SAX cine stack from the base of the heart to the apex.

Strain-Encoding Imaging Analysis

Analysis of SENC images was completed using dedicated software (Myocardial Solutions Myostrain, Morrisville, North Carolina, USA) by a single reviewer *(K.G.D.)*. The SENC images were loaded into the application and the endocardium and epicardium were manually contoured on each image. End diastole and end systole were automatically determined and manually corrected if needed. The contours were automatically tracked throughout the cardiac cycle. The contour tracking was inspected and manually adjusted to ensure optimal tracking. Strain for each segment based on the American Heart Association guidelines is calculated. Circumferential strain is determined using the long axis images (A2C, LVOT, and A4C) (Fig. 2A). Longitudinal strain is determined using the SAX images (base, mid-ventricle, and apex) (Fig. 2B). GCS and GLS are calculated as a mean of all the segments.

Feature-Tracking Analysis

FT analysis was completed using vendor independent, commercially available software (Medis Suite 3.2 QStrain RE, Leiden, the Netherlands) and bSSFP cine images of the A2C, LVOT, A4C, and SAX (base, mid-ventricle, and apex) by a single reviewer *(K.G.D.)*. The endocardium and epicardium were manually contoured on each SAX image. End diastole and end systole were automatically determined and manually corrected if needed. The FT algorithm identifies image characteristics that are trackable frame-by-frame throughout the cardiac cycle. The contours automatically track the endocardium and epicardium throughout the cardiac cycle. The contours were inspected and manually adjusted to ensure optimal tracking. Strain was calculated for each segment according to American Heart Association guidelines. GCS was calculated as a mean of the circumferential strain from each of the 3 SAX images (Fig. 2C). The above process was

Table 1 Baseline characteristics of study population

	Total cohort (N = 134)	Pediatric cohort (N = 89)	ACHD cohort (N = 45)
Male (%)	80 (59.7%)	54 (60.7%)	26 (57.8%)
Age (years)	16.3 (13.7, 19.5)	15.1 (12.4, 16.2)	24.6 (19.5, 33.1)
Height (cm)	165 (153.7, 174)	163 (150, 170)	170 (160, 180)
Weight (kg)	60.8 (49.5, 80)	57.3 (47.2, 72.1)	72.1 (56.7, 92.2)
Body surface area (m^2)	1.7 (1.5, 2.0)	1.6 (1.4, 1.9)	1.9 (1.6, 2.1)
Heart rate (bpm)	80 (68, 93)	85 (72, 95)	74 (66, 87)
Systolic blood pressure (mmHg)	119 (110, 128)	119 (107, 127)	121 (113, 132)
Diastolic blood pressure (mmHg)	69 (63, 78)	67 (63, 77)	74 (65, 79)
Indexed EDV* (mL/m^2)	83.7 (74.2, 95.6)	83.4 (75.0, 93.0)	87.0 (73.5, 98.4)
Indexed ESV* (mL/m^2)	34.5 (29.6, 41.8)	34.5 (28.5, 41.8)	35.4 (31.3, 46.5)
Ejection fraction* (%)	57.0 (54.4, 61.6)	57.3 (54.5, 62.3)	56.9 (53.9, 60.3)

Data presented as N (%) or median (IQR). Adult congenital heart disease (ACHD), end-diastolic volume (EDV), end-systolic volume (ESV)

*Determined from manual planimetry of endocardium of balanced steady-state-free precession cine images in short axis view from base to apex
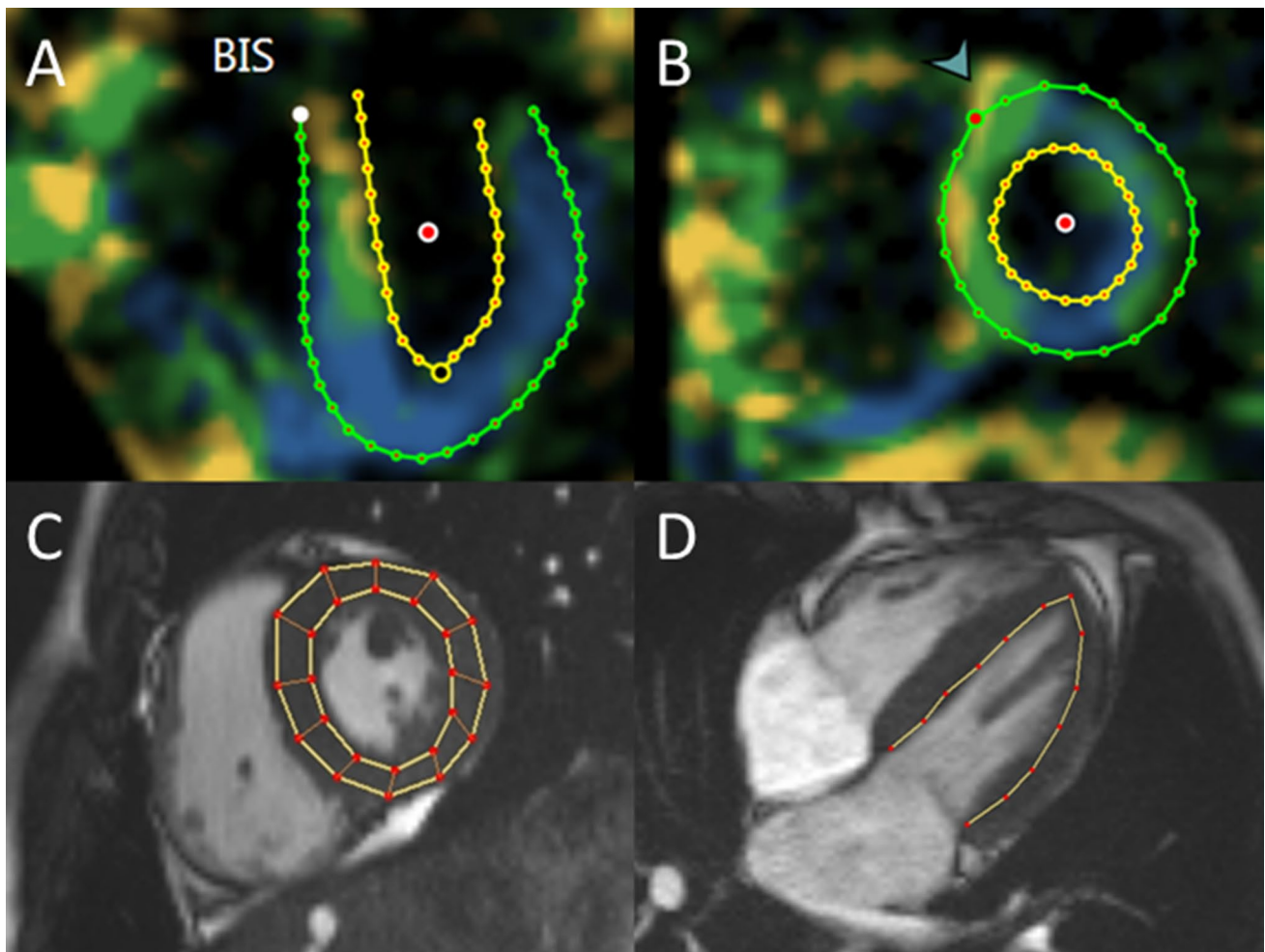

Fig. 2 Example contours for SENC and FT analysis. SENC contours for **A** global circumferential strain and **B** global longitudinal strain. FT contours for **C** global circumferential strain and **D** global longitudinal strain. Strain-encoding magnetic resonance imaging (SENC); feature-tracking (FT)

repeated on the A2C, LVOT, and A4C images in a second session of the QStrain application to calculate GLS. Strain was calculated for each segment according to American Heart Association guidelines. GLS was calculated as a mean of the longitudinal strain from each of the long axis images (Fig. 2D). In addition to the endocardial strain that is the default result, the FT analysis also provides full-thickness myocardial circumferential and longitudinal strain. These FT full-thickness myocardial strain measurements were compared to the respective SENC measurements since SENC derives strain from the entire myocardium.

Late Gadolinium Enhancement Analysis

Late gadolinium enhancement (LGE) images were analyzed by a pediatric cardiologist experienced in CMR as part of clinical care and determined to be positive or negative. LGE quantification was performed with vendor independent, commercially available software (Medis Suite 3.2 QMassMR, Leiden, the Netherlands). Manual planimetry was performed of the LV endocardium and epicardium on the LGE images. LGE quantification was determined using a threshold technique using 5 standard-deviations above the mean signal intensity of normal nulled myocardium. Quantity of LGE was expressed in percentage of total LV myocardial mass.

Intra-Observer Analysis

To assess the reproducibility of the strain analysis techniques, the single reviewer *(K.G.D.)* repeated the SENC and FT GLS and GCS analyses for 15 randomly selected study subjects.

Statistical Analysis

Demographics and clinical characteristics were summarized using descriptive statistics. The median with interquartile range was used to describe continuous variables and *N* (percent) was used to describe categorical variables. Correlation between parameters was assessed by Spearman's rank correlation coefficient (Spearman's ρ). Concordance correlation coefficient and Bland–Altman was used to assess agreement of the two techniques. A simple linear regression was performed to assess the relationship between the two techniques and assess for fixed and proportional bias. With fixed bias, the techniques will differ by a constant degree independent of the value of the measure and is represented by the y-intercept in the linear regression equation. With proportional bias, the difference between the two techniques is proportional based on the values of the measure and is represented by the slope in the linear regression equation. The R^2 from the linear regression was also calculated to determine the proportion of variability explained by the

independent variable. Differences in GLS and GCS based on presence of LGE was evaluated with Mann–Whitney U. Spearman's rank correlation coefficient was used to assess the relationship of GLS and GCS with percent LGE of total LV mass. LGE analysis was restricted to subjects with normal EF (greater than or equal to 55%) as a decrease in GCS and GLS would be expected once EF is abnormal. Intraclass correlation coefficient two-way mixed effects model with absolute agreement was used to assess intra-observer reliability. The primary analysis compared the two methods for the entire cohort. Secondary analyses for the pediatric cohort and the adult congenital heart disease (ACHD) cohort were completed comparing the two methods. An analysis restricted to subjects with structurally normal hearts, who theoretically may have more easily aligned anatomy, was completed to investigate if agreement differed from the total cohort. Additional secondary analyses comparing the SENC GCS and GLS to the FT full-thickness myocardial GCS and GLS was completed for each cohort. To investigate any differences in correlation resulting from the use of two different CMR scanners, subset analysis comparing SENC to FT for GLS and GCS was completed for each scanner. Alpha level of 0.05 or less was pre-specified to indicate statistical significance. All analyses were performed using STATA (version 16; College Station, TX; StataCorp LP).

Results

Study Population

There were 59 structurally normal pediatric subjects, 30 pediatrics subjects with congenital heart disease, and 45 ACHD subjects (Table 2). Clinically measured left ventricular parameters demonstrated normal end-diastolic and end-systolic indexed volumes with normal ejection fraction for the total, pediatric, and ACHD cohorts (Table 1). Eighty-four subjects received contrast with 18 of those having evidence of LGE.

Comparison of SENC and FT

For the total cohort, SENC and FT methods correlated for GLS, and GCS with varying levels of agreement (Table 3A). The correlation and agreement between SENC and FT were stronger for GLS (Fig. 3A & B) than GCS (Fig. 3 C and D). GLS analysis demonstrated a fixed bias of approximately 5% and a mild proportional bias. GCS demonstrated a larger fixed bias of over 10%, with FT numbers tending to be more negative, and a more significant proportional bias, with a smaller difference noted in patients with less negative strain. Similarly, SENC and FT methods correlated for GLS

Table 2 Diagnoses of cohort

	Total (N = 134)	Pediatric (N = 89)	ACHD (N = 45)
Congenital heart disease	75 (56%)	30 (34%)	45 (100%)
Tetralogy of Fallot	29	9	20
Aortic valve abnormality	11	5	6
Aortic arch abnormality	7	3	4
Pulmonary valve abnormality	7	3	4
Pulmonary vein abnormality	6	3	3
d-Transposition of the great arteries	6	2	4
Other	9	5	4
Structurally normal	59 (44%)	59 (66%)	0 (0%)
Control	10	10	0
Muscular dystrophy	14	14	0
Cardiomyopathy	14	14	0
Myocarditis	8	8	0
Arrhythmia	6	6	0
Other	7	7	0

Data presented as *N* (%)

Table 3 Comparison of SENC to feature-tracking analysis of left ventricular function

	SENC	Feature-tracking	Spearman's ρ (p value)	Concordance correlation coefficient (95% CI)
A. Total cohort (N = 134)				
GLS (%)	− 16.7 (− 18.4, − 15.7)	− 21.5 (− 24.0, − 18.8)	0.58 (p < 0.001)	0.24 (0.17–0.31)
GCS (%)	− 17.4 (− 19.0, − 16.1)	− 30.0 (− 34.2, − 25.5)	0.29 (P < 0.001)	0.03 (0.01–0.06)
B. Pediatric cohort (N = 89)				
GLS (%)	− 17.2 (− 18.4, − 15.9)	− 21.3 (− 24.0, − 19.0)	0.51 (p < 0.001)	0.20 (0.11–0.30)
GCS (%)	− 17.5 (− 19.0, − 16.3)	− 29.8 (− 34.5, − 25.2)	0.23 (p = 0.030)	0.03 (0.00–0.05)
C. ACHD cohort (N = 45)				
GLS (%)	− 16.4 (− 18.0, − 14.6)	− 21.6 (− 23.1, − 18.2)	0.74 (p < 0.001)	0.31 (0.19–0.43)
GCS (%)	− 17.1 (− 18.7, − 15.8)	− 30.2 (− 32.9, − 26.1)	0.40 (p = 0.007)	0.05 (0.01–0.08)

Data presented as median (IQR). Strain-encoding magnetic resonance imaging (SENC); global longitudinal strain (GLS), global circumferential strain (GCS), adult congenital heart disease (ACHD)

and GCS for the pediatric (Table 3B) and ACHD cohorts (Table 3C).

Late Gadolinium Enhancement Analysis

Of the 84 subjects who underwent LGE imaging, 18 had evidence of LGE. Eight of the 18 subjects with evidence of LGE and 43 of the 66 subjects without evidence of LGE had an EF greater than or equal to 55%. No difference was seen in SENC GCS, SENC GLS, FT GCS, or FT GLS based on presence of LGE (Table 4). The median percent LGE of total LV mass in subjects with LGE and normal LVEF was 9.9% (IQR 7.8, 16.7). SENC GCS (Spearman's $\rho = 0.03$, $p = 0.829$, SENC GLS (Spearman's $\rho = -0.07$, $p - 0.618$), FT GCS (Spearman's $\rho = 0.10$, $p = 0.475$), and FT GLS (Spearman's $\rho = -0-0.10$, $p = 0.501$) did not correlate with percent LGE of total LV mass for patients with normal LVEF.

Secondary Analyses

SENC and FT methods for GLS and GCS in the structurally normal heart cohorts had similar levels of correlation and agreement to the total cohort (Table 5). SENC GCS correlated to FT full-thickness myocardial GCS with low levels of agreement (Table 6A). Notably, SENC GLS correlated to FT full-thickness myocardial GLS with better levels of agreement (Table 6B). There was a somewhat stronger correlation between SENC and FT for GLS on the Avanto Fit scanner (Spearman's $\rho = 0.67$, $p < 0.0001$) compared to the Avanto scanner (Spearman's $\rho = 0.49$, $p = 0.0001$; however, the concordance correlation coefficients were
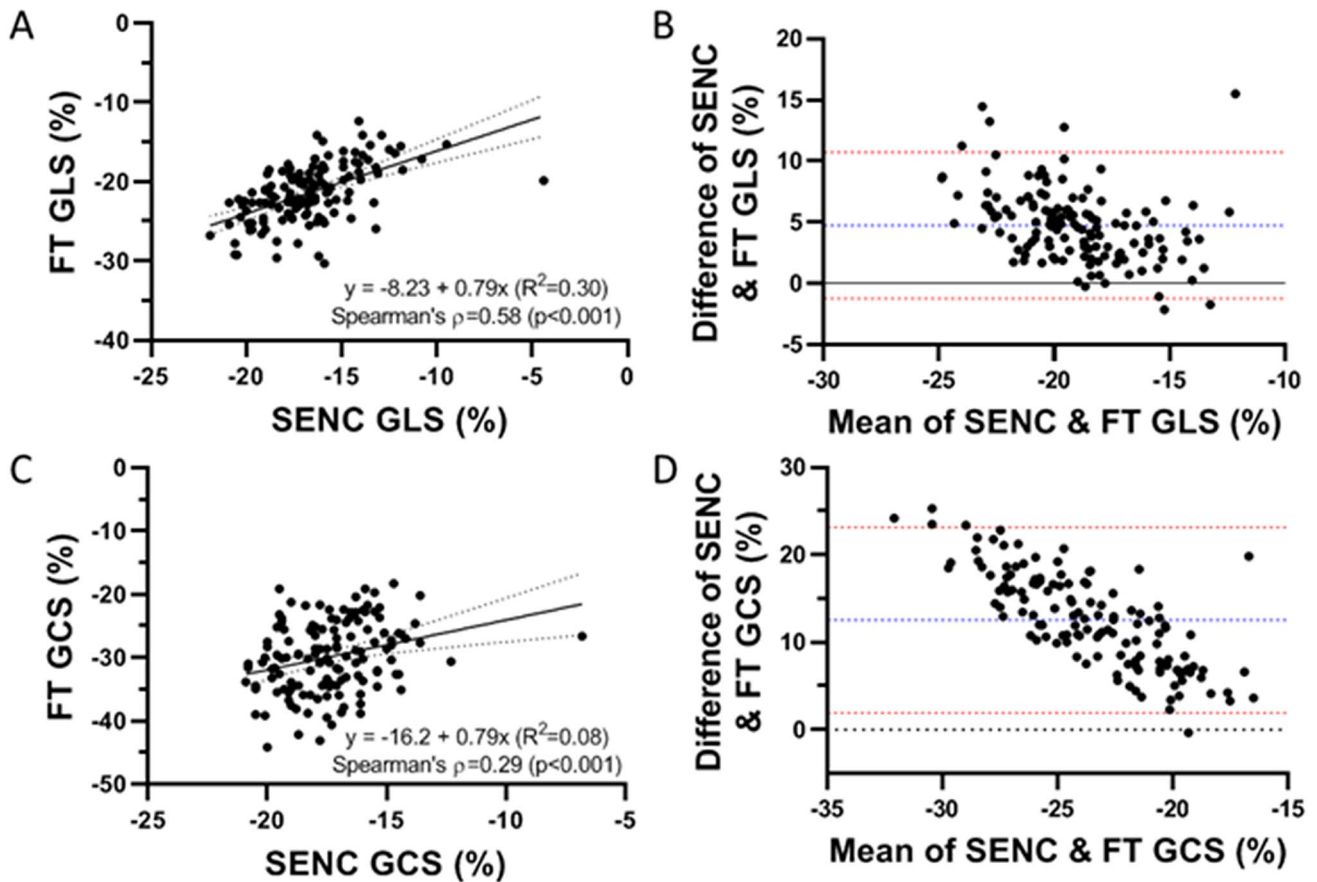
Fig. 3 Comparison of SENC to FT analysis for GLS and GCS for total cohort. GLS **A** correlation with Spearman's ρ and linear regression and **B** Bland–Altman plot. GCS **C** correlation with Spearman's ρ and linear regression and **D** Bland–Altman plot. Strain-encoding magnetic resonance imaging (SENC); feature-tracking (FT); global longitudinal strain (GLS); global circumferential strain (GCS). $N = 134$

Table 4 GLS and GCS comparison with SENC and FT analysis between subjects with normal ejection fraction based on presence of LGE

	LGE positive ($N=8$)	LGE negative ($N=43$)	P value
Ejection fraction (%)	61.0 (57.2, 62.9)	60.2 (56.7, 64.2)	0.970
SENC GCS (%)	-17.8 (-18.7, -15.6)	-17.4 (-19.0, -16.5)	0.854
SENC GLS (%)	-17.6 (-18.4, -16.7)	-17.4 (-18.7, -16.0)	0.661
FT GCS (%)	-31.9 (-35.1, -27.0)	-32.7 (-36.1, -27.6)	0.552
FT GLS (%)	-22.9 (-24.5, -21.9)	-22.6 (-24.6, -19.8)	0.468

Data presented as median (IQR). Global longitudinal strain (GLS); global circumferential strain (GCS); strain-encoding magnetic resonance imaging (SENC); feature tracking (FT); late gadolinium enhancement (LGE)

Table 5 GLS and GCS comparison with SENC and FT analysis in subjects with structurally normal hearts

	SENC	Feature-tracking	Spearman's ρ (p value)	Concordance correlation coefficient (95% CI)
GLS (%)	-17.0 (-18.1, -16.0)	-21.0 (-23.7, -19.0)	0.46 ($p=0.002$)	0.19 (0.08–0.31)
GCS (%)	-17.3 (-19.1, -16.2)	-27.5 (-33.5, -24.2)	0.19 ($p=0.15$)	0.03 (-0.01–0.07)

Data presented as median (IQR). $N=59$. Strain-encoding magnetic resonance imaging (SENC); global longitudinal strain (GLS), global circumferential strain (GCS)

Table 6 Comparison of SENC GCS and GLS to FT full-thickness myocardial GCS and GLS

A	N	SENC GCS (%)	FT full-thickness myocardial GCS (%)	Spearman's ρ (p value)	Concordance correlation coefficient (95% CI)
Total	134	− 17.4 (− 19.0, − 16.1)	− 22.4 (− 25.9, − 18.9)	0.29 (p < 0.001)	0.11 (0.04–0.17)
Pediatric	89	− 17.5 (− 19.0, − 16.3)	− 22.4 (− 26.1, − 18.9)	0.22 (p = 0.041)	0.08 (0.01–0.16)
ACHD	45	− 17.1 (− 18.7, − 15.8)	− 22.6 (− 25.4, − 20.1)	0.45 (p = 0.002)	0.15 (0.04–0.26)
B	N	SENC GLS (%)	FT full− thickness myocardial GLS (%)	Spearman's ρ (p value)	Concordance correlation coefficient (95% CI)
Total	134	− 16.7 (− 18.4, − 15.7)	− 18.7 (− 20.8, − 17.1)	0.62 (p < 0.001)	0.42 (0.31− .052)
Pediatric	89	− 17.2 (− 18.4, − 15.9)	− 18.7 (− 20.9, − 17.0)	0.63 (p < 0.001)	0.38 (0.25–0.52
ACHD	45	− 16.4 (− 18.0, − 14.6)	− 18.6 (− 2.08, − 17.9)	0.62 (p < 0.001)	0.47 (0.31–0.63)

Data presented as median (IQR). Strain-encoding imaging (SENC), global circumferential strain (GCS), feature-tracking (FT), adult congenital heart disease (ACHD)

similar (Table 7). SENC and FT GCS had similar levels of correlation and agreement on the Avanto and Avanto Fit scanners (Table 7). SENC GLS had the strongest intra-rater reliability (ICC 0.99, [0.97–0.99], p < 0.001), followed by SENC GCS (ICC 0.90, [0.73–0.97], p < 0.001), FT GLS (ICC 0.61, [0.15–0.85], p = 0.007) and FT GCS (ICC 0.50, [− 0.05–0.81], p = 0.003).

Discussion

This study is the first of which we are aware to compare SENC and FT in pediatric and ACHD patients. Although the correlation between methods reached statistical significance for all metrics, there was poor agreement between SENC and FT derived GLS and GCS in this cohort of pediatric and ACHD subjects. The agreement between the two methods was better for GLS than GCS, though still poor. The level of agreement of GLS and GCS was similar for the total cohort, pediatric sub-cohort, and ACHD sub-cohort. These findings suggest that GLS and GCS derived from SENC and FT cannot be used interchangeably.

Prior work assessing different techniques to measure strain has demonstrated great disparity in the level of agreement between techniques. Goto et al. demonstrated strong correlation, with limited bias, for GCS measured by DENSE and FT [14]. Augustine et al. found reasonable agreement for GCS, but not GLS, using FT and tagging [11]. However, similar to our findings, correlation with limited agreement between different methods of strain measurement has been the more common finding for both GLS and GCS. This has been demonstrated for FT with SENC, fast-SENC, HARP, tagging and DENSE [12, 13, 15–17]. Additionally, limited agreement has been seen when comparing CMR FT and speckle tracking echocardiography [18, 19]. Amzulescu et al. provide a comprehensive explanation of the numerous factors that lead to variation between methods, including differences in image acquisition, such as spatial and temporal resolution, quality of images, and misalignment between segments, software-based issues resulting from the different

Table 7 Comparison of SENC to FT analysis GLS and GCS based on scanner type

	N	SENC (%)	Feature-tracking (%)	Spearman's ρ (p value)	Concordance correlation coefficient (95% CI)
Avanto GLS	59	− 16.5 (− 17.8, − 14.3)	− 21.7 (− 24.5, − 18.4)	0.51 (p < 0.001)	0.23 (0.13–0.34)
Avanto Fit GLS	75	− 17.0 (− 18.9, − 15.9)	− 21.5 (− 23.7, − 19.3)	0.64 (p < 0.001)	0.24 (0.14–0.34)
Avanto GCS	59	− 17.4 (− 18.3, − 16.1)	− 30.8 (− 34.9, − 27.6)	0.36 (p = 0.005)	0.03 (0.01–0.05)
Avanto Fit GCS	75	− 17.3 (− 19.1, − 16.1)	− 28.6 (− 33.8, − 23.8)	0.30 (p = 0.009)	0.04 (0.01–0.07)

Data presented as median (IQR). Scanner type: Siemens Avanto versus Siemens Avanto Fit. Strain-encoding magnetic resonance imaging (SENC); feature tracking (FT); global longitudinal strain (GLS); global circumferential strain (GCS)

algorithms employed by each vendor, and operator related factors [10].

When applying these principles to our findings, there are a number of hypotheses that can be considered to explain the disagreement observed. Image acquisition parameters differ between the two methods, which could lead to variation in the calculated strain. Specifically, the spatial resolution of the two methods differs and are difficult to directly compare. FT is dependent on the underlying spatial resolution of the cine images, as well as the ability of post-processing software to identify, differentiate, and track regions of tissue. Meanwhile, the prescribed spatial resolution of SENC images on the surface appears lower than typical cine images. But SENC uses tags to obtain strain measurements within each prescribed voxel. This fundamental difference in the method of strain calculation precludes the direct comparison of spatial resolution of the two methods. Additionally, the differences in phase sampling and temporal resolution differs between the two methods, with the SENC images frequently having a lower number of phases. In addition to the imaging parameters, the specific imaging planes of each view likely differs between the two imaging methods. Since SENC uses through-plane tagging, the imaging planes for acquisition are tightly prescribed per sequence recommendations as off-axis acquisition will impact the accuracy of the derived strain. In contrast, the acquisition planes for the bSSFP cines images used in FT analysis were determined by the technicians completing the scan based on standard anatomical landmarks and guidelines. Differences in plane orientation in image acquisition between the two methods can lead to differences in the relationship of myocardial fiber orientation to the direction of strain analysis causing discrepancies in resulting calculations. In addition to the image acquisition, there are differences in the inherent aspects of myocardial deformation interrogation of the two methods. SENC analysis provides an assessment of the deformation of the entire myocardium, while Medis FT software places a greater focus on the endocardium, which may help explain the more negative strain values observed with that technique in our cohort. This is further supported by the improved level of agreement between SENC GLS and FT GLS derived from the full-thickness myocardium, although a similar improvement was not seen for SENC GCS and FT GCS derived from the full-thickness myocardium. Further, the intra-rater reliability must be examined when evaluating the agreement between the two methods as increased intra-rater variance is likely to decrease agreement between methods. SENC had much stronger intra-rater reliability in comparison to FT, which is consistent with prior work [20, 21]. While this study evaluated variability of the software analysis, we were unable to evaluate the effects of image acquisition. Imaging planes have a large effect on SENC and may increase the variability of this modality.

In addition to the cause of the variation between methods, it is important to consider the impact on the usefulness of strain imaging in clinical care. As previously noted, there is significant evidence of the association of alterations in strain with adverse clinical events [1–3, 5, 6]. However, the significant variation in strain between measurement techniques impairs the application of these findings to clinical settings. When extrapolating results of outcome studies to clinical CMRs, care must be taken to ensure that the correct methodologies are used. Standardization between methods and establishment of common normal values are essential for the implementation in everyday clinical care.

A collaborative effort by the American Society of Echocardiography, the European Association of Cardiovascular Imaging, and industry representatives led to the production of a consensus document for the standardization of speckle tracking echocardiography [22]. This document presented recommendations for the definition of measurements, transparency of tracking quality and regularization of tracking, calculation of segmental and global strain values, and reporting of values. A similar effort within CMR may be impeded by the numerous scanner sequences used to obtain images. Despite this additional obstacle, this should be a continued focus of future work to aid in the implementation of CMR based strain techniques in clinical practice.

In addition to evaluating the agreement between strain methods, it is important to consider the ability of strain analysis to identify functional abnormalities of the myocardium. This study evaluated differences in strain in patients with normal LVEF based on the presence or absence of LGE, as well as the correlation between strain values and the percent LGE of total LV mass. None of the strain measurements demonstrated a statistically significant difference based on the LGE status. Additionally, percent LGE of total LV mass did not correlate with any of the strain measurements. It is possible that these results are due to insufficient power from a low number of LGE positive patients in this cohort. This is an area of investigation that should be further explored in future studies with larger cohorts. Additionally, a more targeted approach investigating the association of segmental strain abnormalities with segments with LGE is an area for future investigation.

Limitations

Our cohort was restricted to pediatric and ACHD subjects, which led to a population that was skewed toward adolescents and young adults. Extrapolation of these findings to adult patients without congenital heart disease may not be possible. Additionally, the distribution of left ventricular systolic function was relatively narrow in the cohort, though this is likely a similar distribution to most centers scanning pediatric and adult congenital patients. CMR was completed on two

different scanners during the study period, which introduces the potential for additional variability in our findings. However, the agreement between SENC and FT was similar for both GLS and GCS on sub-analysis based on scanner type. Additionally, this is representative of clinical care where numerous CMR scanners with different parameters are used. Finally, our study used a single reviewer for imaging analysis of both FT and SENC. This may have skewed our results to allow for better correlation between methods. However, using a single reviewer limits variability and allows for more precise assessment of the inherent differences from the techniques themselves.

Conclusions

SENC and FT derived GLS and GCS correlated with poor agreement in a cohort of pediatric and ACHD patients, suggesting that SENC and FT cannot be used interchangeably for diagnosis or prognosis. CMR physicians must take care when interpreting and applying strain cut-offs from the literature to use identical methodology. Standardization of CMR strain is necessary to accelerate the clinical adoption of strain.

Data Availability The datasets generated during and/or analyzed during the current study are available from the corresponding author on reasonable request.

Code Availability Not applicable.

Declarations

Conflict of interest The authors declare that they have no competing interests. Myocardial solutions provided analysis software but had no input into design of study, analysis, or interpretation.

Ethical Approval The study was approved by the Vanderbilt University Medical Center Institutional Review Board (IRB #161524).

Consent to Participate For all pediatric subjects, guardians provided informed consent and the subject provided assent. All adult subjects provided informed consent.

Consent for Publication Not applicable.

References

1. Buss SJ, Breuninger K, Lehrke S, Voss A, Galuschky C, Lossnitzer D, Andre F, Ehlermann P, Franke J, Taeger T, Frankenstein L, Steen H, Meder B, Giannitsis E, Katus HA, Korosoglou G (2015) Assessment of myocardial deformation with cardiac magnetic resonance strain imaging improves risk stratification in patients with dilated cardiomyopathy. Eur Heart J Cardiovasc Imaging 16:307–315

2. Diller GP, Kempny A, Liodakis E, Alonso-Gonzalez R, Inuzuka R, Uebing A, Orwat S, Dimopoulos K, Swan L, Li W, Gatzoulis MA, Baumgartner H (2012) Left ventricular longitudinal function predicts life-threatening ventricular arrhythmia and death in adults with repaired tetralogy of fallot. Circulation 125:2440–2446

3. Moon TJ, Choueiter N, Geva T, Valente AM, Gauvreau K, Harrild DM (2015) Relation of biventricular strain and dyssynchrony in repaired tetralogy of fallot measured by cardiac magnetic resonance to death and sustained ventricular tachycardia. Am J Cardiol 115:676–680

4. Poterucha JT, Kutty S, Lindquist RK, Li L, Eidem BW (2012) Changes in left ventricular longitudinal strain with anthracycline chemotherapy in adolescents precede subsequent decreased left ventricular ejection fraction. J Am Soc Echocardiogr 25:733–740

5. Romano S, Judd RM, Kim RJ, Kim HW, Klem I, Heitner JF, Shah DJ, Jue J, White BE, Indorkar R, Shenoy C, Farzaneh-Far A (2018) Feature-tracking global longitudinal strain predicts death in a multicenter population of patients with ischemic and nonischemic dilated cardiomyopathy incremental to ejection fraction and late gadolinium enhancement. JACC Cardiovasc Imaging 11:1419–1429

6. Saito M, Negishi K, Eskandari M, Huynh Q, Hawson J, Moore A, Koneru S, Foster S, Marwick TH (2015) Association of left ventricular strain with 30-day mortality and readmission in patients with heart failure. J Am Soc Echocardiogr 28:652–666

7. Suerken CK, D'Agostino RB Jr, Jordan JH, Melendez GC, Vasu S, Lamar ZS, Hundley WG (2020) Simultaneous left ventricular volume and strain changes during chemotherapy associate with 2-year postchemotherapy measures of left ventricular ejection fraction. J Am Heart Assoc 9:e015400

8. Claus P, Omar AMS, Pedrizzetti G, Sengupta PP, Nagel E (2015) Tissue tracking technology for assessing cardiac mechanics: principles, normal values, and clinical applications. JACC Cardiovasc Imaging 8:1444–1460

9. Osman NF, Sampath S, Atalar E, Prince JL (2001) Imaging longitudinal cardiac strain on short-axis images using strain-encoded MRI. Magn Reson Med 46:324–334

10. Amzulescu MS, De Craene M, Langet H, Pasquet A, Vancraeynest D, Pouleur AC, Vanoverschelde JL, Gerber BL (2019) Myocardial strain imaging: review of general principles, validation, and sources of discrepancies. Eur Heart J Cardiovasc Imaging 20:605–619

11. Augustine D, Lewandowski AJ, Lazdam M, Rai A, Francis J, Myerson S, Noble A, Becher H, Neubauer S, Petersen SE, Leeson P (2013) Global and regional left ventricular myocardial deformation measures by magnetic resonance feature tracking in healthy

volunteers: comparison with tagging and relevance of gender. J Cardiovasc Magn Reson 15:8

12. Bucius P, Erley J, Tanacli R, Zieschang V, Giusca S, Korosoglou G, Steen H, Stehning C, Pieske B, Pieske-Kraigher E, Schuster A, Lapinskas T, Kelle S (2019) Comparison of feature tracking, fast-SENC, and myocardial tagging for global and segmental left ventricular strain. ESC Heart Fail 7:523

13. Cao JJ, Ngai N, Duncanson L, Cheng J, Gliganic K, Chen Q (2018) A comparison of both DENSE and feature tracking techniques with tagging for the cardiovascular magnetic resonance assessment of myocardial strain. J Cardiovasc Magn Reson 20:26

14. Goto Y, Ishida M, Takase S, Sigfridsson A, Uno M, Nagata M, Ichikawa Y, Kitagawa K, Sakuma H (2017) Comparison of displacement encoding with stimulated echoes to magnetic resonance feature tracking for the assessment of myocardial strain in patients with acute myocardial infarction. Am J Cardiol 119:1542–1547

15. Ibrahim EH, Stojanovska J, Hassanein A, Duvernoy C, Croisille P, Pop-Busui R, Swanson SD (2018) Regional cardiac function analysis from tagged MRI images. Comparison of techniques: Harmonic-Phase (HARP) versus Sinusoidal-Modeling (SinMod) analysis. Magn Reson Imaging 54:271–282

16. Ohyama Y, Ambale-Venkatesh B, Chamera E, Shehata ML, Corona-Villalobos CP, Zimmerman SL, Hassoun PM, Bluemke DA, Lima JAC (2015) Comparison of strain measurement from multimodality tissue tracking with strain-encoding MRI and harmonic phase MRI in pulmonary hypertension. Int J Cardiol 182:342–348

17. van Everdingen WM, Zweerink A, Nijveldt R, Salden OAE, Meine M, Maass AH, Vernooy K, De Lange FJ, van Rossum AC, Croisille P, Clarysse P, Geelhoed B, Rienstra M, Van Gelder IC, Vos MA, Allaart CP, Cramer MJ (2018) Comparison of strain imaging techniques in CRT candidates: CMR tagging, CMR feature tracking and speckle tracking echocardiography. Int J Cardiovasc Imaging 34:443–456

18. Orwat S, Kempny A, Diller GP, Bauerschmitz P, Bunck A, Maintz D, Radke RM, Baumgartner H (2014) Cardiac magnetic resonance feature tracking: a novel method to assess myocardial strain. Comparison with echocardiographic speckle tracking in healthy volunteers and in patients with left ventricular hypertrophy. Kardiol Pol 72:363–371

19. Pryds K, Larsen AH, Hansen MS, Grondal AYK, Tougaard RS, Hansson NH, Clemmensen TS, Logstrup BB, Wiggers H, Kim WY, Botker HE, Nielsen RR (2019) Myocardial strain assessed by feature tracking cardiac magnetic resonance in patients with a variety of cardiovascular diseases - a comparison with echocardiography. Sci Rep 9:11296

20. Korosoglou G, Gitsioudis G, Voss A, Lehrke S, Riedle N, Buss SJ, Zugck C, Giannitsis E, Osman NF, Katus HA (2011) Strain-encoded cardiac magnetic resonance during high-dose dobutamine stress testing for the estimation of cardiac outcomes: comparison to clinical parameters and conventional wall motion readings. J Am Coll Cardiol 58:1140–1149

21. Feisst A, Kuetting DLR, Dabir D, Luetkens J, Homsi R, Schild HH, Thomas D (2018) Influence of observer experience on cardiac magnetic resonance strain measurements using feature tracking and conventional tagging. Int J Cardiol Heart Vasc 18:46–51

22. Voigt JU, Pedrizzetti G, Lysyansky P, Marwick TH, Houle H, Baumann R, Pedri S, Ito Y, Abe Y, Metz S, Song JH, Hamilton J, Sengupta PP, Kolias TJ, d'Hooge J, Aurigemma GP, Thomas JD, Badano LP (2015) Definitions for a common standard for 2D speckle tracking echocardiography: consensus document of the EACVI/ASE/Industry Task Force to standardize deformation imaging. J Am Soc Echocardiogr 28:183–193